ELSEVIER

Contents lists available at ScienceDirect

## Journal of Materials Research and Technology

journal homepage: www.elsevier.com/locate/jmrt



# Microstructure and machinability of selective laser melted titanium alloy in micro-milling



Muhammad Rehan, Te Zhao, Wai Sze Yip\*, Sandy Suet To\*\*

State Key Laboratory of Ultra-precision Machining Technology, Department of Industrial and Systems Engineering, The Hong Kong Polytechnic University, Hung Hom, Kowloon, Hong Kong

#### ARTICLE INFO

Handling editor: P Rios

Keywords:
Selective laser melting
Micro milling
Microstructure
Titanium alloys
Machinability
Machining dynamics

#### ABSTRACT

This study thoroughly investigates the relationship between the microstructure of Selective Laser Melted (SLM) Ti6Al4V and improved machinability in micro-milling. The study demonstrates a detailed comparison of grain structure and crystallographic orientation through electron backscatter diffraction and phase mapping with experimental analysis, highlighting the fine, needle-like and acicular  $\alpha'$  martensite of SLM Ti6Al4V and the larger, equiaxed  $\alpha$  grains with intergranular  $\beta'$  phase of wrought Ti6Al4V, has a significant impact on machinability in micro-milling. The exceptional resistance to deformation of SLM microstructure resulting from its inherent hardness and decreased ductility, leads to reduced tool interaction in micro-milling. In contrast, the wrought material exhibits larger grains, which result in greater ploughing, increased burr formation, and significant tool wear. The reduction in burr width on the down-milling side for SLM Ti6Al4V at a feed rate of 1  $\mu$ m/tooth can reach up to 71.6%. Furthermore, the surface finish of SLM Ti6Al4V is consistently superior to wrought Ti6Al4V in term of surface roughness, emphasizing the microstructural advantages of SLM titanium alloys for machinability. The findings of this study offer a comprehensive understanding of the positive effect of microstructure of SLM titanium alloys on machining performance in micro-milling.

### 1. Introduction

Additive manufacturing (AM) has emerged as a highly promising technology with extensive research and application prospects, particularly in aerospace, biomedicine, and precision engineering. However, despite its potential, the widespread adoption of AM in these fields encounters various challenges that need to be addressed. These challenges encompass concerns related to irregular surface topography, inadequate surface roughness, limited dimensional accuracy, and suboptimal microstructure and mechanical properties of the printed components [1, 2]. Selective laser melting (SLM), a popular technique for metal additive manufacturing, offers several advantages i.e., rapid production, a variety of material options, direct production with computer-aided design, adaptability to intricate geometries, and the ability to form internal structures [3-5]. However, parts produced using SLM exhibit relatively unsatisfactory surface quality, necessitating additional machining processes to achieve the desired surface integrity [6,7]. This highlights the need for a comprehensive understanding of the interaction between the SLM process parameters and the resulting surface characteristics [6].

With the increasing demand for miniature components, micro milling has become a commonly used machining technology in precision industries. It offers high accuracy, enabling the handling of complex 3D features with minimal material loss. However, machining of micro-scale components introduces its own set of challenges, such as tool deflection, surface quality, and chip evacuation [8–11].

Titanium (Ti) alloys are widely utilized in aerospace, precision engineering, and medical device sectors for their outstanding corrosion resistance, biocompatibility, and high temperature resistance [12–14]. The properties of Ti6Al4V alloy produced by AM differ significantly from those made through traditional methods i.e., forging and casting [15–17]. SLM fabricated Ti–6Al–4V is characterized by  $\alpha'$  martensite with a hexagonal closed-packed structure, resulting from the rapid cooling that transforms the stable  $\beta$  phase into  $\alpha'$  martensite [4]. Contrary, conventionally manufactured Ti6Al4V displays equiaxed  $\alpha$  grains and intergranular  $\beta$  phases, with directional alignment due to deformation in processes like forging. Traditional methods lead to coarser grains because of the slower cooling rates, which permit more grain growth [5]. The directional and rapid solidification process in SLM,

E-mail addresses: lenny.ws.yip@polyu.edu.hk (W.S. Yip), sandy.to@polyu.edu.hk (S.S. To).

<sup>\*</sup> Corresponding author.

<sup>\*\*</sup> Corresponding author.

coupled with the substantial temperature gradient during the molten pool surface formation, significantly contributes to the anisotropic behaviour of the material [18,19]. Columnar grain growth along specific directions, such as the (100) orientation aligned with the maximum heat extraction direction, leads to a substantial heterogeneous and anisotropic microstructure [20-23]. A location-specific thermal history is established due to the thermal gradient between the melt pool and previously solidified layers [23,24]. Lower ultimate tensile stress and yield stress but higher elongation are observed along the longitudinal direction compared to the transverse direction. This behavior can be attributed to the presence of elongated  $\alpha$  phase grains forming along the boundaries of the preceding  $\beta$  grains, serving as weak junction points [22]. To overcome the inherent challenges associated with AM-produced components, post-processing heat treatments are typically implemented to stabilize the microstructure, alleviate thermal stresses, reduce porosity, and improve the mechanical properties of the as-built parts [4,25]. The machinability of components fabricated using AM technologies has received significant attention in metal machining research due to better mechanical properties as compared to prepared by forging or rolling [26]. But it shows deviations from specified surface finish and geometric tolerances required for critical and precision applications [4,26]. There is a need of post-processing of as-fabricated components to overcome the limitations in achieving the desired surface finish and dimensional accuracy using current AM technology [27].

The machinability of a material is directly influenced by its mechanical properties, which are in turn determined by the manufacturing method and the resulting microstructural development 5,28. Various studies have been conducted to investigate how manufacturing methods, and consequently the microstructure, affect precision machining. Sharma et al. [29] explored how microstructural features, such as grain size, phase fraction, and morphology, impact the machining characteristics and tool wear in high-speed machining of Ti–6Al–4V, revealing a significant correlation with cutting forces, sub-surface changes, and wear patterns. Airao et al. [3] compared the

micro-milling outcomes of SLM-produced Ti6Al4V with its wrought counterpart, finding that the wrought alloy, with its equiaxed grains, exhibited more adhesive wear, built-up edge (BUE) formation, and poorer surface finish. In contrast, the SLM Ti6Al4V, characterized by a lamellar structure and increased hardness, experienced reduced tool wear and BUE, albeit with higher surface roughness due to abrasion. The microstructure of components manufactured using AM, specifically SLM, is critical due to its direct correlation with the mechanical properties required for advanced applications. Microstructural heterogeneity, such as columnar grain orientation and  $\alpha'$  martensite distribution, can impact micro-milling performance, affecting cutting forces, tool wear, and surface integrity. This necessitates a thorough understanding of the relationship between SLM process parameters, resulting microstructure, and micro-milling performance. This study thoroughly investigates the impact of microstructural characteristics, such as grain orientation and crystallographic texture, on the high-speed micro-end milling of Ti6Al4V fabricated using SLM and wrought processes. The research meticulously characterizes microstructural features and disorientation angles using advanced techniques such as scanning electron microscopy (SEM) and electron backscatter diffraction (EBSD). The study systematically evaluates the impact of different feed rates on tool life, chip formation dynamics, and surface topography. The schematic of this study is shown in Fig. 1.

#### 2. Methodology

#### 2.1. Specimen preparation

Two test samples were prepared for conducting experiments, one via Selective Laser Melting (SLM) and the other as a wrought titanium alloy (Table 1). Both samples were standardized at 25 mm  $\times$  25 mm x 25 mm for consistent comparison. The SLM process utilized powder with a size range of 15–53  $\mu$ m, and the printing parameters included a laser power of 340W, a scanning speed of 1250 mm/min, a hatch spacing of 0.3 mm,

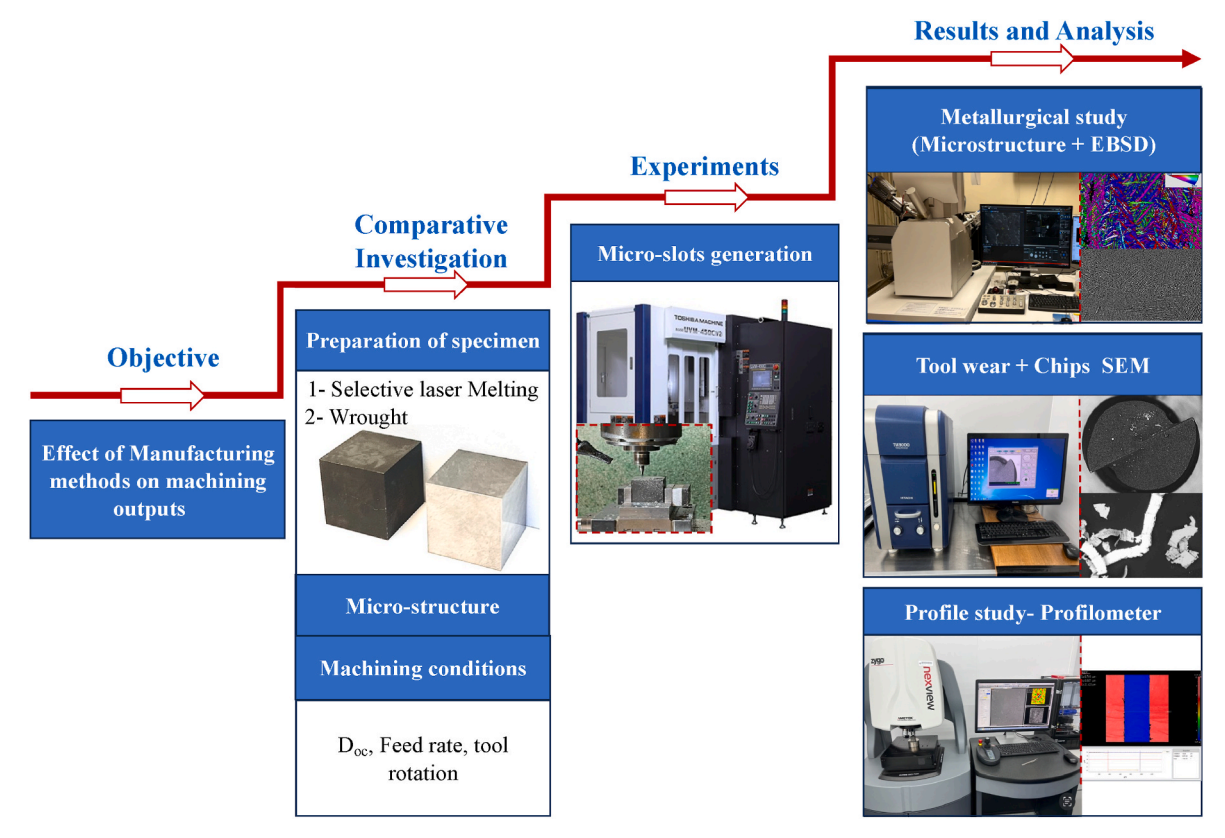


Fig. 1. The schematic of this study.

Table 1
Composition of wrought and Ti6Al4V fabricated by AM.

Element		Ti	Al	V	Fe	С	0	N	Н
Percentage composition	Wrought	Balance	6.28	4.05	0.18	0.032	0.159	0.006	0.0021
	AM	Balance	6.01	4.08	0.042	0.006	0.097	0.005	0.003

and a layer thickness of 60  $\mu m$ . Following printing, vacuum annealing at 800 °C for 3 h in an argon atmosphere was performed to refine the microstructure and mitigate residual stresses, ensuring unbiased machining outcomes. The titanium samples were sourced from Firmakes Titanium Co., Ltd., with each material presenting distinct microstructures evident in EBSD patterns. Microstructural and EBSD analyses were executed using a TESCAN MIRA microscope and an Oxford Instruments Nordlys Max3, respectively. EBSD parameters were set at 20.0 kV acceleration voltage, a 70.0° sample inclination, and a sampling rate of 638.40 Hz. Sample preparation involved grinding and electropolishing with a solution of 5% perchloric acid and 95% glacial acetic acid at 10 °C, under 60V for 30 s. The EBSD raw data was then processed with EDAX-TSL's Aztec Crystal software for enhanced data clarity and interpretation.

#### 2.2. Experimental setup

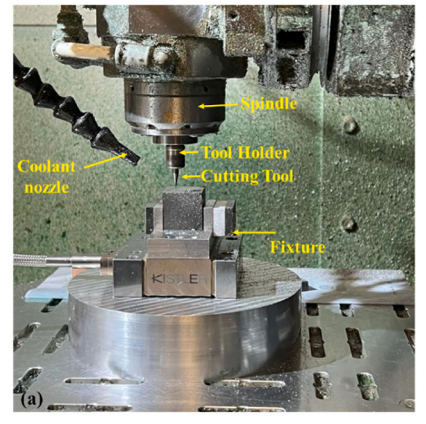
The experiments were carried out on a Toshiba UVM-450C(V2) fiveaxis machining center, with a resolution of 0.01  $\mu m$  in the X, Y, and Z axe. Fig. 2 represents the experimental setup and the cutting profiles on the part surface. The experiments are conducted at four different feed rate levels, ranging from 1 to 4  $\mu$ m/tooth with 1  $\mu$ m intervals, while maintaining a constant tool rotation speed of 65,000 rpm and a depth of cut of 15 µm. CBN micro-end milling tools were used and fabricated by Changzhou Easy Joint Imports and Exports Co. Ltd., with a 600 µm cutting diameter. These tools featured a total length of 50 mm, a cutting length of 1.5 mm, a shank diameter of 4 mm, a neck diameter of 0.55 mm, a 3 µm cutting edge radius, and a helix angle of 30°. To maintain experimental consistency, a new tool was utilized for each sample. Beforehand, the workpiece was prepared with a 2 mm diameter end mill to establish a uniform surface and eliminate oxide layers. The coolant of choice was Klubercut CO (6-102), a biodegradable vegetable oil, to enhance machining conditions. Surface roughness and topography were measured using an optical profiling system (Zygo NexviewTM), while the tool edge, machined surface, and chip geometry were examined using a Hitachi tabletop microscope (TM3000). Surface roughness of each groove was evaluated using a non-contact measurement method with the optical profiling system. Five readings were taken along the center line of each groove, and the average value is taken.

#### 3. Results and discussion

#### 3.1. Microstructure, grain structure and orientation

Fig. 3 showcases the microstructural and Electron Backscatter Diffraction (EBSD) analysis of both SLM Ti6Al4V and wrought specimens. The SLM Ti6Al4V in Fig. 3a exhibits the microstructures with free of pores, keyholes, and fusion defects, indicative of excellent quality and near-complete density of the samples. The micrograph highlights  $\beta$  grain boundaries demarcated by dashed lines, within which acicular  $\alpha'$ martensite is embedded. This structure forms due to the rapid thermal cycling of approximately 104-105 K/s during SLM, fostering a unique microstructure [30-32]. The SEM images in (Fig. 3b) reveal needle-like  $\alpha'$  phases with grain sizes around 50-80  $\mu m$ , alongside laminar structures averaging 40-60 µm, dispersed in a hexagonal closed-packed matrix, characteristic of a supersaturated solid solution [33,34], leading to the martensitic transformation within the columnar crystals [35]. These martensites, varying in size and exhibiting a large aspect ratio, are dispersed across the primary  $\beta$  grains, as depicted in Fig. 3b. In the following cycle, when temperatures exceed the phase transition range, primary  $\alpha'$  reverts to  $\beta$  and liquid phases. As temperatures fall below the martensite start temperature (Ms), the liquid transforms back to primary acicular  $\alpha'$ , and the remaining  $\beta$  phase converts to secondary acicular  $\alpha'$ and tertiary acicular  $\alpha$ ' [36,37]. Due to the high and rapid cooling rates, a hierarchy of martensitic structures forms, including primary, secondary, and tertiary  $\alpha'$  martensite, which are distinguished and labeled in Fig. 3b [36]. Further it can be seen that the orientation of the  $\alpha'$ martensite is either parallel or perpendicular to each other, with the primary acicular  $\alpha'$  phase appearing as long columnar structures, while the secondary and tertiary phases are progressively finer. At higher magnification, as shown in Fig. 3b, the hierarchical martensitic structure becomes evident, with primary, secondary, and tertiary  $\alpha'$  phases, each with distinct sizes and orientations, reflecting the influence of SLM process parameters [37]. The  $\beta$  phase (traces), observable as brighter regions along  $\alpha'$  boundaries due to its higher vanadium content, contributes to the complexity of the microstructure [7,38,39]. The rapid cooling in the SLM process also retains  $\beta$  phase remnants at  $\alpha$  grain boundaries, fostering a microstructure conducive to enhanced mechanical properties.

The microstructure in SLM Ti6Al4V features a combination of



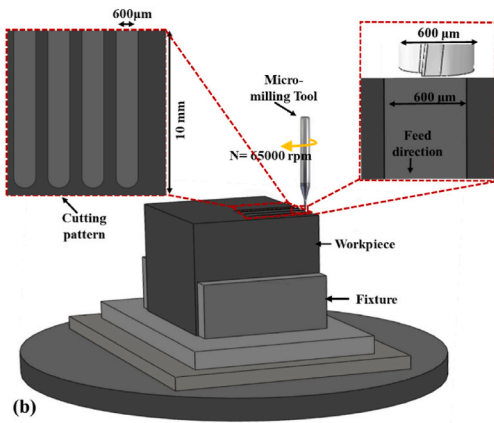


Fig. 2. Experimental setup; (a) micro milling setup, (b) cutting profiles and details.

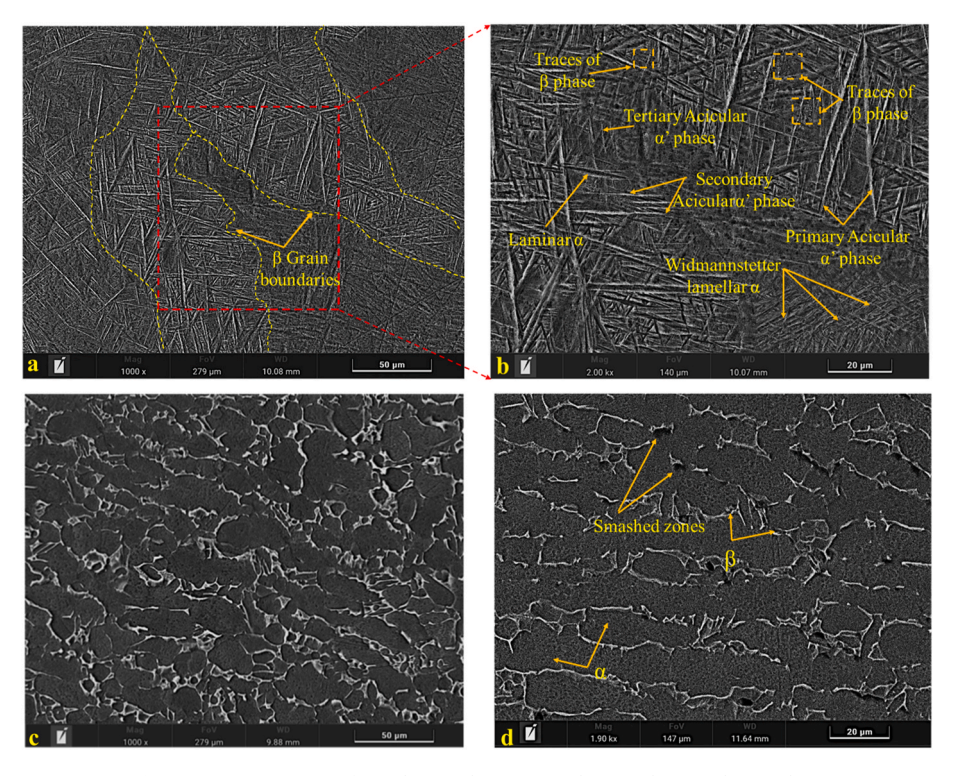


Fig. 3. Microstructures of Ti6Al4V: (a-b) SLM Ti6Al4V, (c-d) wrought Ti6Al4V.

acicular  $\alpha'$  martensite, as seen in (Fig. 3b), the Widmanstätten structure, which forms under specific cooling conditions, with  $\alpha$  laths growing within  $\beta$  grains [40–43]. The fine  $\alpha/\alpha'$  microstructure is responsible for the enhanced tensile strength and toughness of SLM Ti6Al4V, highlighting its superior mechanical integrity [44,45]. Further hexagonal close packed  $\alpha$  in SLM Ti6Al4V reduces its ductility [46]. This detailed analysis underscores the intricate relationship between the SLM process, microstructure, and the resultant mechanical properties of the material.

Contrasting with the SLM sample, the wrought Ti6Al4V has a different grain growth pattern. Fig. 3(c&d) illustrates the microstructure of wrought Ti6Al4V, featuring equiaxed  $\alpha$  grains, recognizable as dark regions, amidst a matrix that includes intergranular  $\beta$  phases, appearing as luminous zones along grain boundaries. This combination forms a characteristic bimodal structure, a result of controlled phase transformation during hot deformation [47]. The  $\beta$ -to- $\alpha$  transformation, governed by diffusion processes, takes place within the  $\alpha + \beta$  phase field at temperatures beneath the  $\beta$ -transition point [48–50], shaping the microstructure and, consequently, the mechanical properties of alloy. The wrought material exhibits  $\alpha$  grains with an average size of approximately 20 µm, larger than the 14 µm reported by Shunmugavel et al. [48], highlighting the influence of processing conditions. The  $\alpha$  and β phases adhere to Burger's orientation relationship, with their crystallographic planes and directions aligning in a specific manner during phase transitions, underscoring the material's structural complexity [9, 51-53].

The EBSD analysis in (Inverse Pole Figures (IPF//Z) and grain boundaries (GB) maps in Fig. 4 provide a clear distinction between the microstructural arrangements of wrought and SLM Ti6Al4V. The phase mapping reveals a uniform grain structure without any blank or dark regions, indicating a defect-free analysis and the absence of zero solutions, thereby confirming EBSD data. The phase mapping of both samples representing grain orientation and phase distribution show that there are no blank or dark regions throughout the regions, which shows absence of defects.

For SLM Ti6Al4V the Inverse Pole Figure (IPF) maps display grains sharing similar crystallographic orientations, with color gradients from

blue to red indicating a progression from smaller to larger grain sizes in Fig. 4a. The average grain length (measured) is approximately 23 μm, ranging up to 75 µm, highlighting a spectrum of grain sizes. SLM microstructures predominantly feature grains colored blue, green, or red in IPFs, corresponding to surface normal [01-10], [-12-10], and [0001], respectively. These grains exhibit elongated forms, with some broader sections, with the majority falling within the 15-25 µm range. Thicknesses vary from 0.5 to 3.5 µm. The aspect ratio, a crucial metric for grain morphology, is consistently above 1, indicative of an elongated grain structure, with some grains reaching an aspect ratio of 20, while the average is around 11. This contrasts with the findings of Vranken et al. [40], they noted columnar martensite growth in SLM parts, highlighting the impact of microstructure on micro milling forces. The wrought material (Fig. 4d), lacking the SLM-specific textures, presents a more random crystallographic distribution and larger grain sizes, emphasizing the profound impact of manufacturing techniques on phase distribution and microstructural characteristics.

Ti-6Al-4V, a dual-phase alloy, owes its mechanical properties to the  $\alpha$  and  $\beta$  phases. The  $\alpha$  phase, dominant in strength and creep resistance, contrasts with the  $\beta$  phase's softer characteristics. The unique processing histories of SLM and wrought materials, including thermal cycles and cooling rates, shape their microstructures differently. SLM, with its rapid cooling, favors the  $\alpha$  phase, as seen in Fig. 5a, with 99.7%  $\alpha$  and a mere 0.3% β phase. Conversely, wrought Ti6Al4V, shown in Fig. 5b, has a more balanced distribution with 6.3%  $\beta$  and 93.7%  $\alpha$  phases. The Widmanstätten structure, which forms under specific cooling conditions, with  $\alpha$  laths growing within  $\beta$  grains [40–43]. This structure, with an average size of 2.3  $\mu$ m and a phase composition of approximately 95%  $\alpha$ and 5%  $\beta$ , significantly impacts ductility and toughness [41,54]. This difference stems from the thermal dynamics and microstructural evolution unique to each manufacturing process. Rapid cooling of SLM inhibits  $\beta$  phase development, promoting a finer grain structure that discourages  $\beta$  phase at grain boundaries. Residual stresses and defects further contribute to phase composition of SLM. Fig. 5c and d shows disorientation angle distribution of SLM and wrought Ti6AL4V. On the other hand, the disorientation angle quantifies the angular deviation

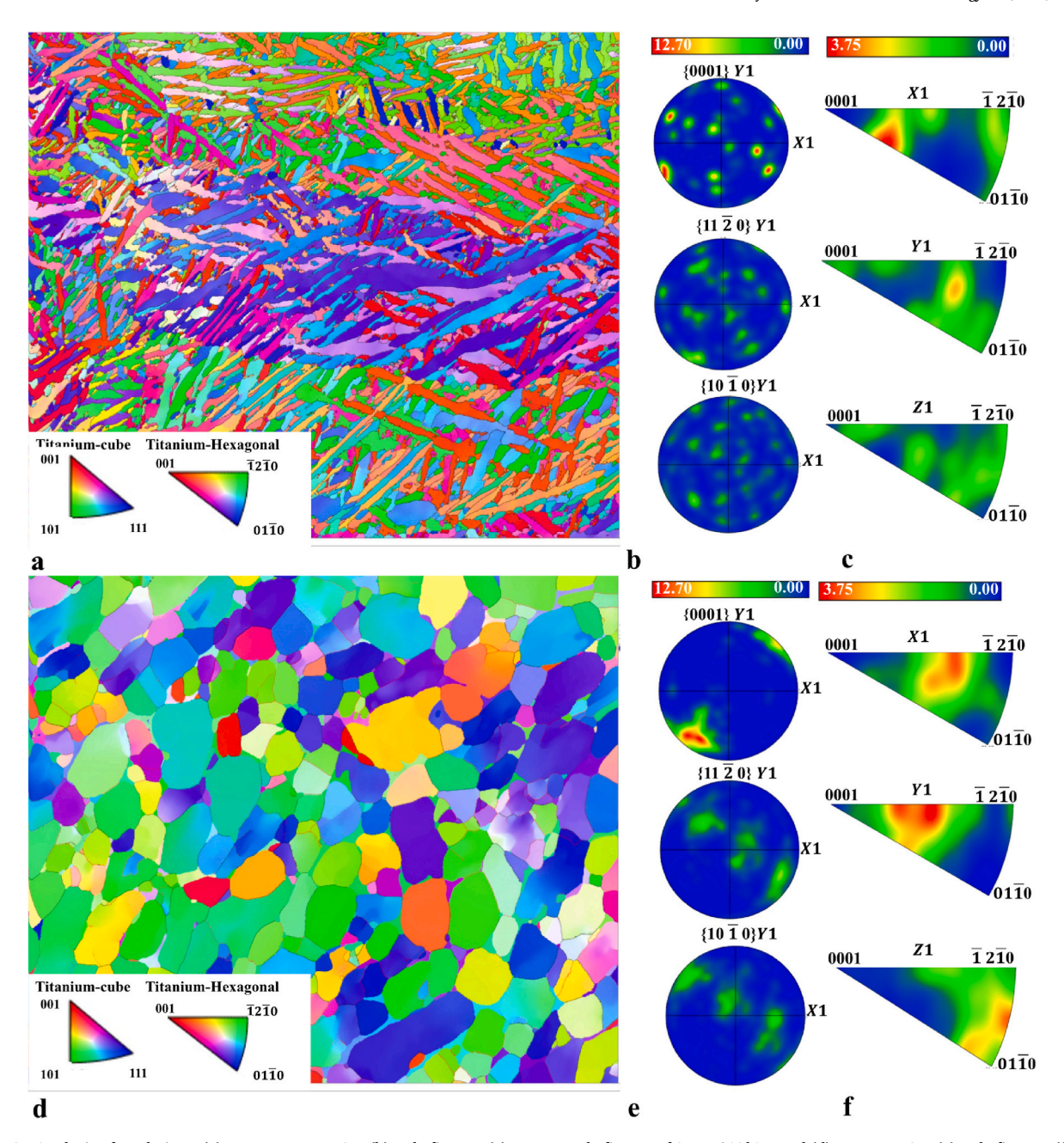


Fig. 4. EBSD Analysis of workpiece: (a) IPF maps//Z + GB, (b) Pole figures, (c) Inverse pole figures of SLM Ti6Al4V; and (d) IPF//Z + GB, (e) Pole figures, (f) Inverse pole figures of Wrought Ti6Al4V.

between neighboring grains in a material, serving as an indicator of grain boundary characteristics. High disorientation angles, particularly those over 15°, denote high-angle grain boundaries, which are pivotal in influencing grain growth, recrystallization, and the material's mechanical properties [22,55]. In the case of SLM Ti6Al4V, the distribution of disorientation angles is skewed towards larger angles, most of the adjacent laths tended to have the high-angle grain boundaries of in the range of 55°, 60° or 65° which led to the distinct difference and regularity in the color of the  $\alpha'$  laths in the IPF map offering the identification of primary  $\beta$  boundaries suggesting substantial intergranular rotations due to rapid solidification and a complex microstructure [56]. This pattern is evident in the theoretical, neighbor pair, and random pair distributions, with the latter two highlighting the dominance of high-angle grain boundaries and the influence of the bcc- $\beta$  to hcp  $\alpha'$ phase transformation and acicular  $\alpha'$  martensite [56,57]. Conversely, wrought Ti6Al4V displays a more varied disorientation angle

distribution, encompassing both low and high angles, with a noticeable frequency of higher angles in theoretical distributions. This diversity reflects the material's exposure to deformation processes during manufacturing, which induce a range of crystallographic orientations [22,56]. Neighbor pair distributions in wrought Ti6Al4V reveal a balance of low-angle and high-angle grain boundaries, with a tendency towards lower angles, indicative of the diverse grain shapes and orientations resulting from conventional deformation. Random pair distributions span a broad spectrum of angles, mirroring the more traditional microstructure formed through deformation and recrystallization processes.

#### 3.2. Tool wear

The microstructural attributes of the workpiece, encompassing grain size, orientation, and disorientation angle distribution, play a crucial

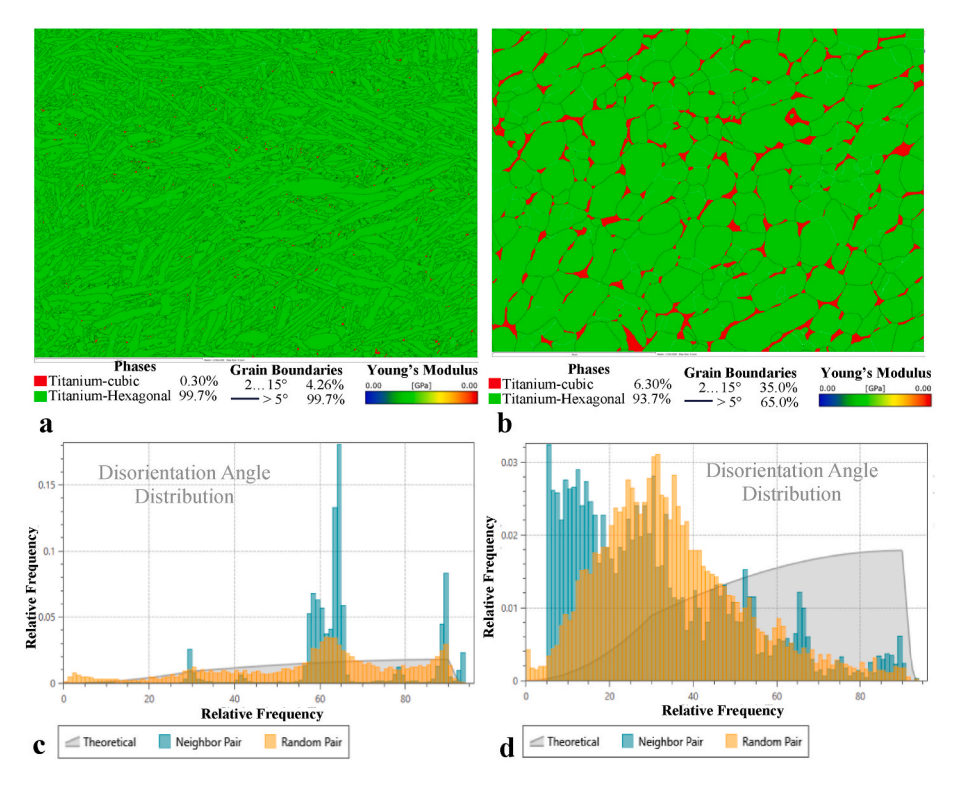


Fig. 5. Phase mapping: (a) SLM Ti6Al4V, (b) Wrought Ti6Al4V, Disorientation angle distribution: (c) SLM Ti6Al4V, (d) Wrought Ti6Al4V.

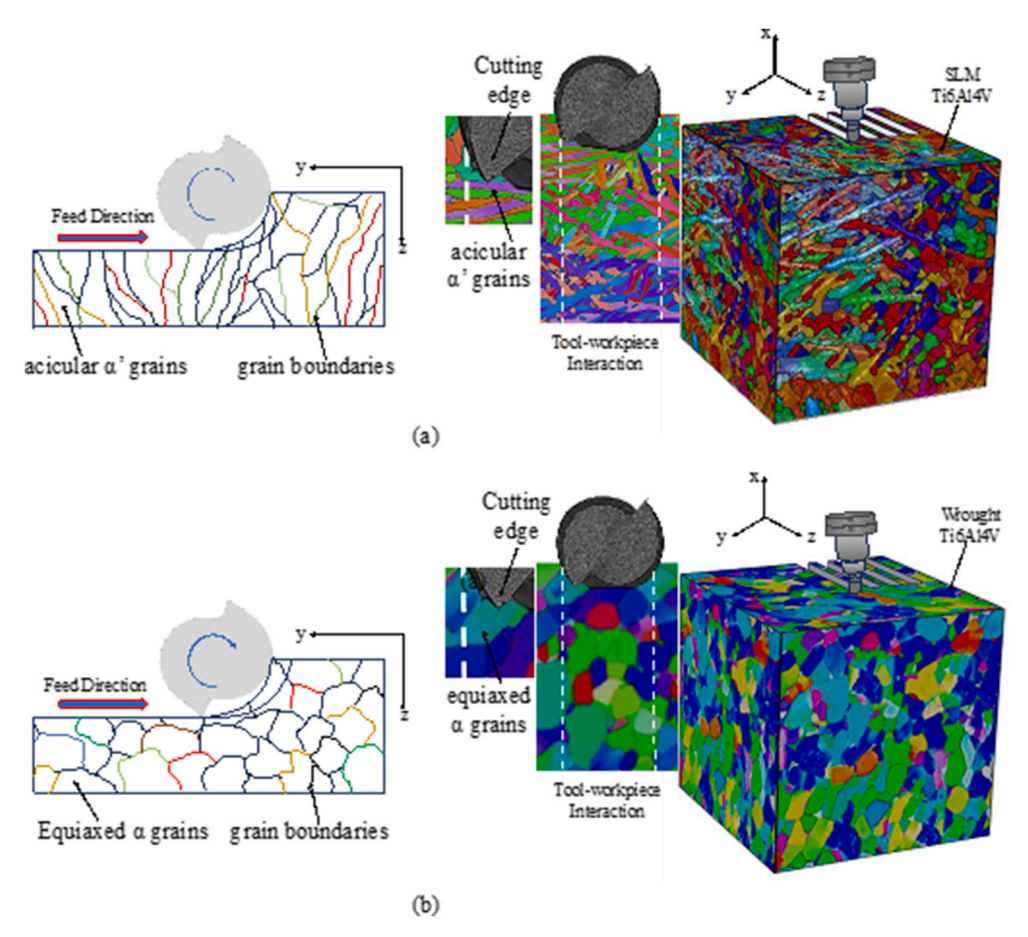


Fig. 6. The effect of tool workpiece interaction on grains of the machined surface; (a) SLM Ti6Al4V, (b) Wrought Ti6Al4V.

role in dictating the efficacy and results of micro-milling operations. Fig. 6 visually represents these microstructural variations, highlighting their significance. These variations critically influence parameters such as surface finish, cutting force dynamics, tool degradation, chip morphology, and the stability of the machining process [58,59]. The distribution of disorientation angles between grains directly impacts the material response to machining heat and mechanical stress, thereby affecting heat dissipation, surface integrity, tool life, and dimensional precision. A profound comprehension of these microstructural influences is vital for refining micro-milling strategies and attaining high-precision manufacturing goals. As illustrated in Fig. 6, the schematic demonstrates how grain orientation relative to the tool edge influences machining across different regions. The SLM Ti6Al4V exhibits lower ductility compared to its wrought counterpart. Grain boundary density, calculated as the ratio of the total grain boundary perimeter to the examined area, significantly impacts the machining process. The theory of shear banding, where the cutting action is guided, reveals that substantial changes in grain orientation relative to the shear plane lead to variations in grain boundary density, which in turn, influences the machining dynamics significantly [60,61].

Scanning Electron Microscopy (SEM) images captured at various magnifications and perspectives, including cross-sections, rake, and flank faces of the cutting tools, are presented in Fig. 7, revealing distinct wear patterns. Both tools exhibit wear mechanisms primarily characterized by abrasion and adhesion. A close examination of the crosssectional views (Fig. 7a and d) reveals minimal wear initially, with adhesive wear evident due to the interaction between the tool and workpiece surfaces. During the machining process, workpiece material tends to adhere to the tool edges due to friction. Notably, Fig. 7b highlights a more substantial adhesive layer of wrought Ti6Al4V material on the cutting edge compared to SLM Ti6Al4V as shown in Fig. 7e, indicating a higher tendency for adhesion. This phenomenon is attributed to the machining conditions, where temperatures can reach between 450 and 650 °C, promoting adhesion at the tool-workpiece interface [62,63]. The wrought material, with its equiaxed microstructure and a larger  $\boldsymbol{\beta}$  grain fraction, is more susceptible to deformation under high pressure and temperature, facilitating adhesion layers. Conversely, the SLM

material's higher hardness and thinner grains resist adhesion, with its lower ductility promoting grain detachment rather than adhering to the tool. Ahmadi et al. [64] support these findings, emphasizing the impact of microstructure on micro-milling wear. The detachment of adhered material during further machining can lead to edge degradation, compromising tool sharpness. The non-uniform grain structure and larger grain sizes in wrought Ti6Al4V contribute to uneven wear patterns. The distribution of grain disorientation angles in wrought Ti6Al4V, with a broad range of low and high-angle boundaries, complicates the machining dynamics. Low-angle boundaries can concentrate stresses locally, exacerbating tool wear, while the diverse grain orientations introduce complexity in wear patterns, underscoring the importance of considering microstructural characteristics in tool wear analysis and micro-milling process optimization.

For both milling tools, welded chips, or Built-Up Edge (BUE), are evident, but the tool rake face processed on wrought Ti6Al4V (Fig. 7c) shows a more substantial BUE layer. This phenomenon is due to microstructural differences, particularly the presence of the  $\beta$  phase in wrought material, which, under the heat of machining, softens and adheres more readily to the tool compared to the SLM counterpart. The work by Sharma and Meena [29] underscores how work material microstructure critically affects BUE formation in micro-machining. The SLM Ti6Al4V, with its higher hardness and laminar grain structure, exhibits less ductility, which inhibits extensive plastic deformation and thus BUE buildup, as shown in Fig. 7f. As the machining progresses, adhered particles from wrought Ti6Al4V are prone to chip off the tool surface, causing surface degradation. This adhesion leads to an increase in the edge radius, shifting the material removal mechanism from efficient shearing to less desirable ploughing. Ploughing disrupts the chip flow, causing it to bypass the enlarged edge, exacerbating wear through continuous contact. The dominant wear mechanisms for wrought Ti6Al4V thus involve adhesion, abrasion, and edge chipping. In contrast, SLM Ti6Al4V, with its characteristic larger α colonies and microstructural partitioning, exhibits lower yield stress, reducing the tendency for tool chipping. The rapid solidification in SLM contributes to a more uniform microstructure with better grain boundary distribution. This homogeneity promotes more controlled material removal, reducing the

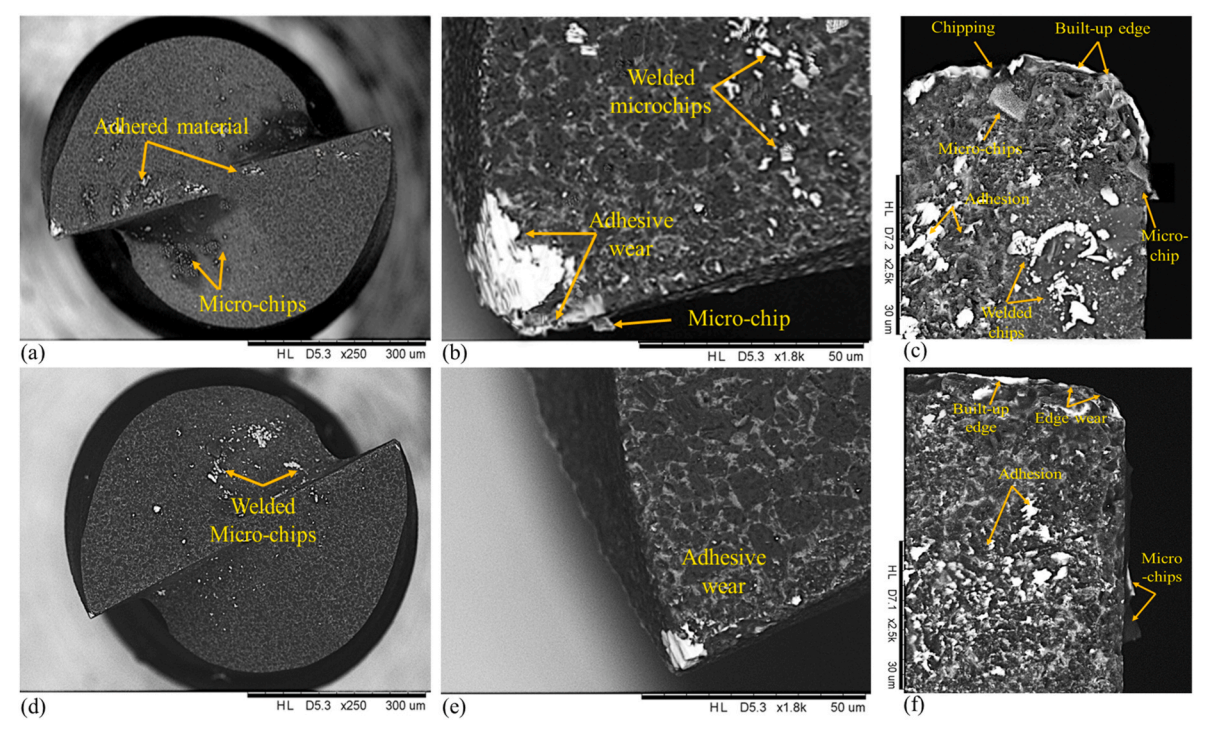


Fig. 7. Tool wear after milling of: (a-c) wrought Ti6Al4V, (d-f) SLM Ti6Al4V.

likelihood of BUE formation and contributing to a more favorable tool condition during machining. The smoother material response in SLM Ti6Al4V is a testament to the influence of the manufacturing process on tool-life and machining efficiency.

The influence of Selective Laser Melting (SLM) on the machining dynamics of Ti6Al4V during micro-milling is a critical area of study, especially regarding tool wear. As an additive manufacturing process, SLM imparts unique microstructural characteristics to Ti6Al4V, which significantly affect its machining behaviour. The microstructure of SLMproduced Ti6Al4V often exhibits anisotropy and residual stresses, as the above section mentioned, which can alter the dynamics of the micromilling process. Additionally, features such as fine grains, porosity, and distinct phase distributions, which differ from those in conventionally manufactured Ti6Al4V, are common. These microstructural attributes can lead to variations in mechanical properties, such as hardness and ductility, which in turn influence machining dynamics. As a result, there can be variations in cutting forces, vibrations, and thermal loads during machining. These factors complicate the dynamic interaction between the tool and the workpiece, potentially leading to increased tool wear.

#### 3.3. Chips morphology

Fig. 8 presents SEM images of chips generated from micro-milling experiments on wrought and SLM Ti6Al4V under varying cutting conditions, with Fig. 8(a-d) showcasing wrought and Fig. 8(e-h) SLM material. The chip morphology exhibits clear variations in response to different machining settings. Both materials form lamella structures on the free surface, while contact surfaces display gouging marks, indicative of hard material interaction. The lamella, a result of phase property disparities, contrasts with the marks from localized stress. Increasing the feed rate from 1 to 4  $\mu$ m/tooth significantly alters chip morphology. For wrought Ti6Al4V, as shown in Fig. 8a-d, higher feed rates (3-4 µm/ tooth) yield shorter chips with lateral cracks, suggesting severe plastic deformation under high forces and temperatures. Lower feed rates (1-2 μm/tooth) produce chips with serrated edges but without central cracks, pointing to less intense deformation conditions. SLM Ti6Al4V chips, as shown in Fig. 8(e-h), are generally longer and narrower, attributed to the lamellar microstructure's resistance to deformation compared to the more ductile, broader chips from wrought material, which owe their shape to the high elongation of equiaxed grains. Despite length

reduction in chips with increased feed rate, SLM chips maintain a more consistent shape with fewer serrations, a result of the material's higher hardness and unique thermal behavior, which mitigates against excessive softening during machining. Notably, adhered micro-particles are evident on the surfaces of wrought Ti6Al4V chips, as shown in Fig. 8 (a–d), a consequence of its microstructure promoting surface softening and adhesion. Conversely, the SLM Ti6Al4V's lamellar structure, with reduced ductility and toughness, inhibits material adherence to the chip surface, highlighting the influence of microstructure on chip formation and surface interactions during the micro-milling process.

#### 3.4. Surface quality

To facilitate accurate measurement, the top burr width (both down milling and up milling) was measured and analyzed in this experiment. A consistent area at the top of the milled groove, where burrs were uniformly generated, was selected for detection. The top burr width was measured multiples times at various positions, and the final value was determined by calculating the average of these repetitions. Burr size was measured for each case as the feed rate varied, with the average size for each slot presented in Fig. 9a and b for up milling side and down milling sides respectively. A general trend was observed: as the feed rate increased, the burr size decreased, reaching a minimum at a feed rate of 4  $\mu$ m/tooth. As the feed rate increases, the cutting mechanism transitions from shearing to ploughing, where the material is plastically deformed rather than cut off [5], this trend is shown in Fig. 9c. At  $F_r =$ 1μm/tooth, for SLM TI6Al4V the average burr width of up milling side is 49.3% less than wrought Ti6Al4V whereas for the down milling side the difference is around 71.6%.

Fig. 10 presents SEM images that contrast burr formation during micro-milling of wrought Ti6Al4V and SLM Ti6Al4V at a feed rate of  $1\mu m/tooth$ . A clear distinction is observed, with burrs on the down-milling side consistently larger than those on the up-milling side for both materials. Notably, SLM Ti6Al4V exhibits smaller burr heights compared to wrought Ti6Al4V. This disparity stems from the micro-structural differences: SLM Ti6Al4V's acicular  $\alpha'$  martensite within an hcp matrix promotes a harder, more brittle structure, facilitating clean breakage during machining, as reported in literature [33,34]. The material resistance to deformation contributes to reduced burr formation. In contrast, wrought Ti6Al4V, characterized by equiaxed  $\alpha$  grains and intergranular  $\beta$  phases, undergoes increased plastic deformation,

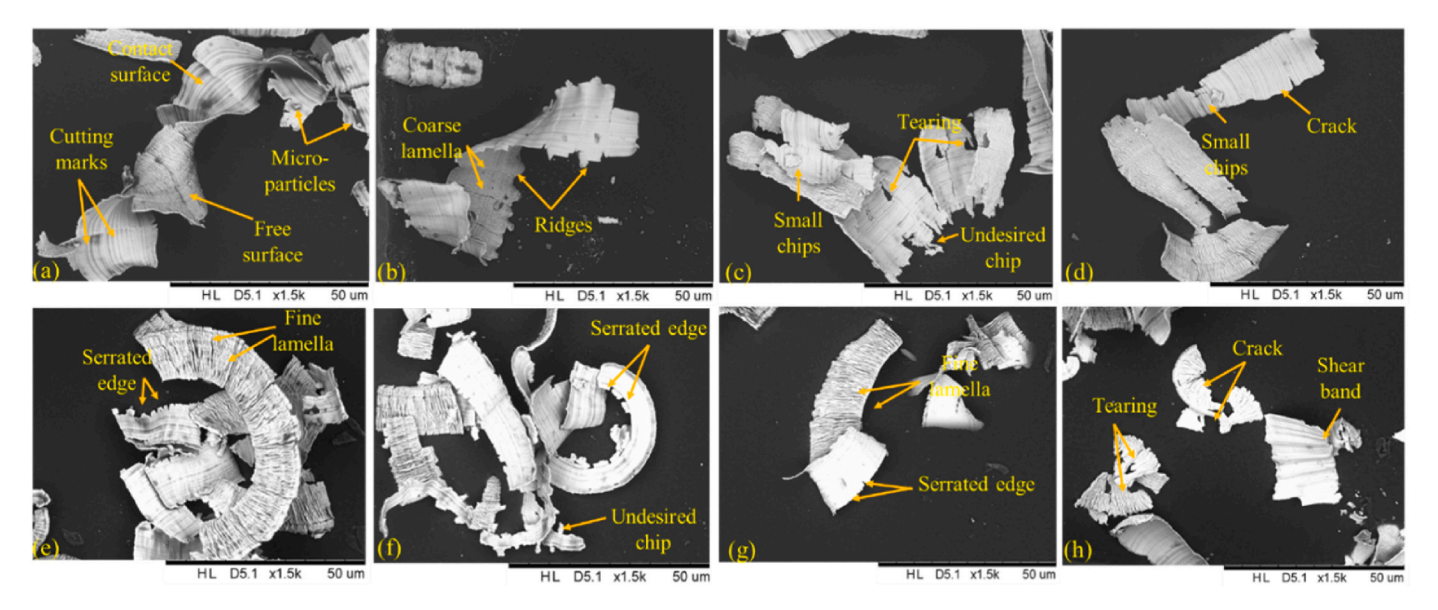


Fig. 8. Chips morphology at different feed rate: wrought Ti6Al4V (a) 1μm/tooth, (b) 2μm/tooth, (c) 3μm/tooth, (d) 4μm/tooth; SLM Ti6Al4V (e) 1μm/tooth, (f) 2μm/tooth, (g) 3μm/tooth, (h) 4μm/tooth.

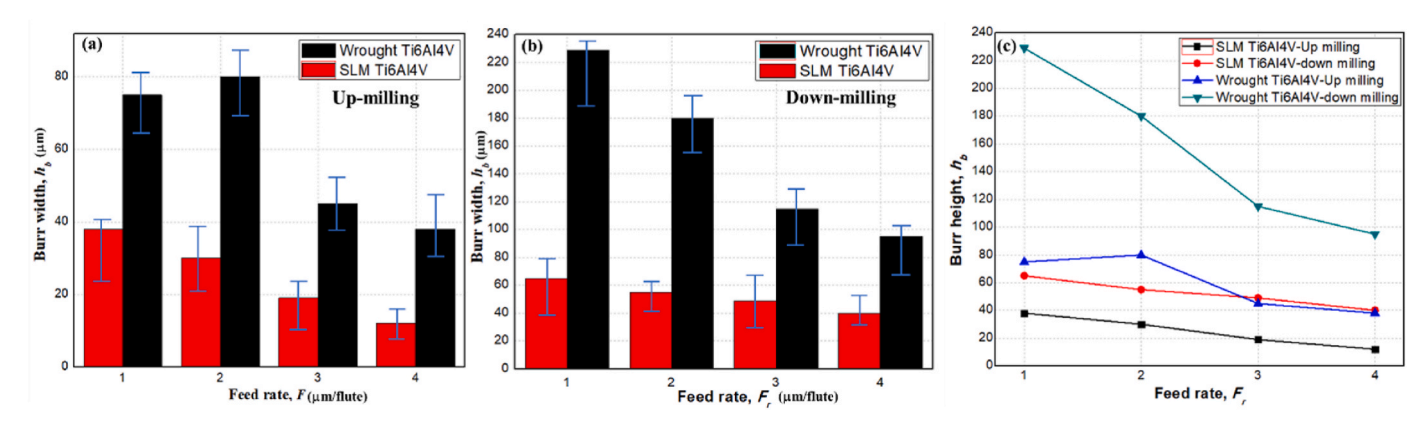


Fig. 9. (a) Measurement of burr heights for up milling sides, (b) Measurement of burr heights for down milling sides, (c) Change of burr heights as a function of Fr.

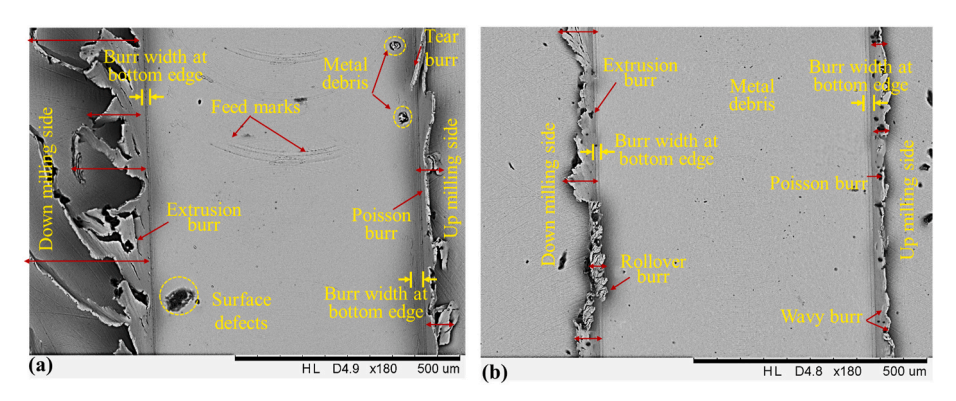


Fig. 10. SEM images of burr formation at machined slots at 1μm/tooth; (a) wrought Ti6Al4V, (b) SLM Ti6Al4V.

leading to larger burrs due to the material's capacity for flow under stress [5]. The lower hardness of wrought Ti6Al4V enables greater ploughing at lower feeds, exacerbating burr formation, a phenomenon echoed by Nakayama et al. [65] and Airao et al. [3]. The latter authors specifically highlighted the role of ductility, with wrought Ti6Al4V equiaxed grains promoting wider and thicker burrs due to extensive shear deformation. Chen et al.[66] further support this analysis, emphasizing that the reduced ductility and enhanced hardness of SLM Ti6Al4V minimize shear deformation, thus producing smaller burrs. The key factor here is the material response to machining stress, with AM Ti6Al4V unique microstructure, resulting from the SLM process, leading to a reduced tendency for plastic deformation and, consequently, smaller burrs upon detachment. Also, burr formation in machining is categorized into distinct types, including Poisson burrs, roll-over burrs, tear burrs, and cut-off burrs. Poisson burrs arise from compressive stresses, roll-over burrs from the bending of residual chips, and tear burrs from material tearing rather than clean shearing. Fig. 10 presents a detailed analysis of burr formation on wrought Ti6Al4V, highlighting extrusion burrs caused by the cutting-edge pressure. On the up-milling section, the specimen displays tear and Poisson burrs, indicative of localized stress and material failure modes. In comparison, SLM Ti6Al4V shows a different pattern, with wavy Poisson burrs on the up-milling side and a combination of extrusion and roll-over burrs on the down-milling side, influenced by the cutter's helix angle and the mechanics of material removal. The presence of bottom edge burrs, related to the tool ploughing effect and adhesive interactions, is a common issue in both materials, particularly evident during transitions from up-to down-milling. These burrs can be mitigated by enhancing the tool interaction with the workpiece and minimizing ploughing effects. SEM images in Fig. 10 further illustrate the contrast between the wrought and SLM samples. The wrought Ti6Al4V shows clear feed marks, a result of built-up edges and microchipping on the tool, which, upon detachment,

leave metal debris due to the  $\beta$ -phase's temperature-induced softening. Conversely, the SLM Ti6Al4V surface is devoid of such marks and debris, suggesting a cleaner machining process, likely attributed to its unique microstructure and higher resistance to adhesion. This comparison underscores the importance of understanding the material microstructure in predicting and controlling burr formation and surface quality in micro-milling operations.

The surface profile curves presented in Fig. 11 further substantiate the preceding discussion, illustrating how surface morphology varies at different transverse positions due to instantaneous tool-workpiece interactions. As the tool rotates, the instantaneous undeformed chip thickness fluctuates, causing the material removal process to alternate between ploughing and shearing [67]. The central surface profile is smooth and consistent, while the profiles near the edges (cut-in and cut-out sides) exhibit irregularities and waviness. During the middle stage of the cutting process, increased instantaneous undeformed chip thickness leads to shearing and cutting actions being the dominant material removal modes, resulting in a smooth, uniform surface profile with low peaks. Conversely, during the cut-in and cut-out stages, the surface profile shows many irregularities due to ploughing and material accumulation from the middle portion. Additionally, these undulations are denser in wrought material, whereas they are more uniform and comparatively less dense in SLM material.

A comparison at a feed rate of 1  $\mu$ m/tooth reveals marked disparities in surface finish. SLM Ti6Al4V yields a notably smoother surface, free of defects, in contrast to wrought Ti6Al4V, which exhibits surface imperfections, debris, and distinct feed marks, as shown in Fig. 10. Surface roughness shown in Fig. 12 of the machined surface confirms this distinction, with SLM Ti6Al4V achieving a consistently smoother range of 19.5–52.1 nm, outperforming wrought Ti6Al4V, which ranges from 23.2 to 56.9 nm. Fig. 12 plots surface roughness against feed rate, illustrating a trend where an initial increase in feed rate from 1 to 2  $\mu$ m/

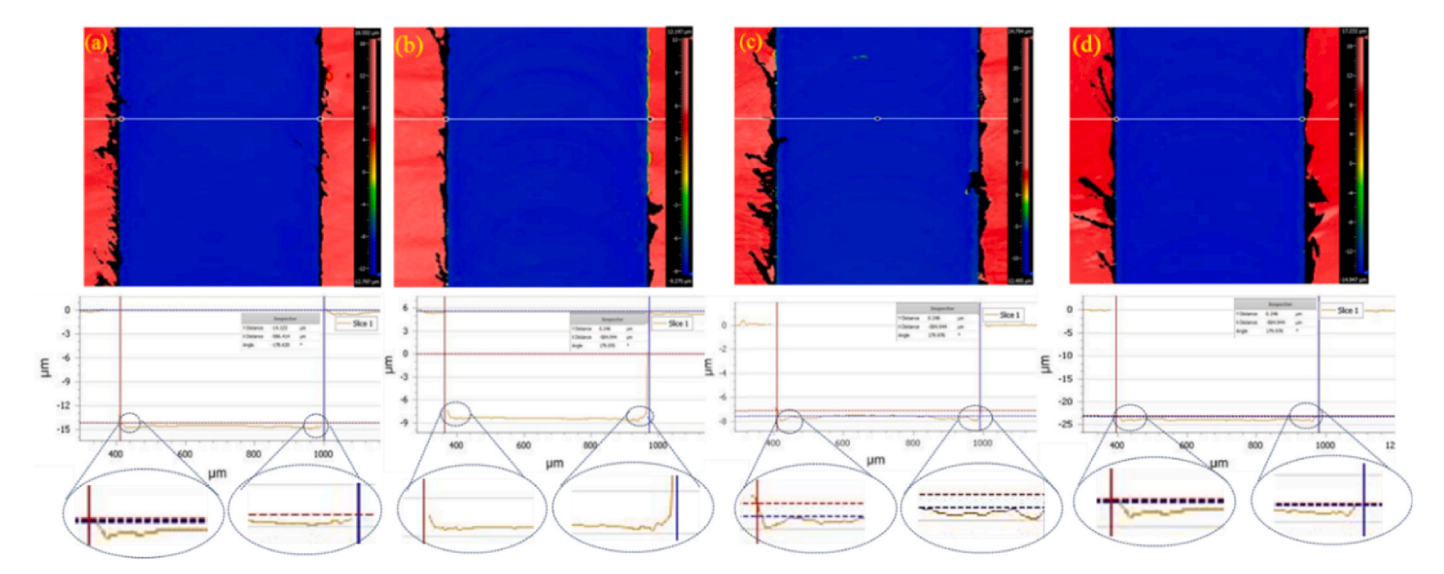


Fig. 11. Surface profile of the machined slots: (a) SLM at  $F_r = 1 \mu m/tooth$ , (b) SLM at  $F_r = 4 \mu m/tooth$ , (c) Wrought at  $F_r = 1 \mu m/tooth$ , (d) Wrought at  $F_r = 4 \mu m/tooth$ .

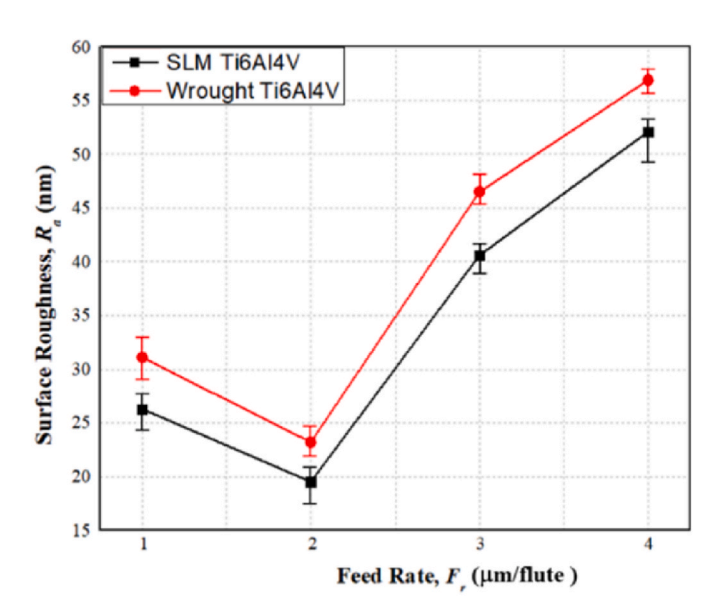


Fig. 12. Surface Roughness of the machined slots of SLM and wrought Ti6Al4V at different feed rates.

tooth yields a decrease in roughness, reaching minimum values of 19.5 nm for SLM and 23.2 nm for wrought material. This improvement is attributed to reduced ploughing effects at these intermediate feed rates. However, beyond 2 µm/tooth, surface roughness escalates due to a shift towards less controlled mechanisms, such as extrusion and non-shear actions, leading to instability. Specifically, from 2 to 4 µm/tooth, surface roughness experiences a substantial increase of 62.57% for SLM and 59.22% for wrought Ti6Al4V, highlighting the critical role of feed rate in determining surface finish quality. This analysis aligns with the work of Airo et al. [68] and Chen et al. [69], who emphasize that at low feeds, ploughing exacerbates adhesion and burr formation, while higher feeds lead to surface degradation through increased adhesion and visible feed marks. The enhanced surface finish of SLM Ti6Al4V is directly linked to its microstructural characteristics, including higher hardness and lower ductility, which minimize lateral deformation and contribute to a superior finish. This finding aligns with the study of Ji et al. [6] on Inconel 718, where SLM processing resulted in improved surface roughness due to controlled grain structure, a feature not as effectively replicated in wrought materials. Specifically, at a feed rate of 1 µm/tooth, SLM

Ti6Al4V presents a clean surface, while the wrought material shows defects, emphasizing the microstructure's influence on surface quality. The graph in Fig. 12 underscores the initial improvement and subsequent deterioration of surface roughness with increasing feed rates, underscoring the delicate balance required in feed selection for optimal micro-milling outcomes. The heightened sensitivity to feed rates in micro-milling, as noted by Chen et al. [69], further supports the need for precise control, particularly in SLM Ti6Al4V, where microstructure refinement plays a pivotal role in achieving high-quality finishes.

#### 4. Conclusions

The SLM-produced Ti–6Al–4V alloy has a distinct microstructure dominated by  $\alpha'$  martensite, which transforms the  $\beta$  phase into a hexagonal close-packed structure. The mechanical properties of the alloy are inextricably linked to its microstructure, which varies greatly depending on the manufacturing method. This comprehensive study combines SEM and EBSD techniques with experiment analysis to investigate tool wear, chip morphology, and surface finish, demonstrating the variations in machineability caused by distinct microstructural features. The research findings and implications are as follows.

- 1. SLM yields needle-like  $\alpha'$  martensite and laminar grains in a controlled matrix, while wrought Ti6Al4V features equiaxed  $\alpha$  grains with intergranular  $\beta$  phases, showing a broader range of grain orientations. SLM Ti6Al4V has a high  $\alpha$  phase concentration with minimal  $\beta$ , unlike wrought Ti6Al4V, which balances  $\alpha$  and  $\beta$  phases. These microstructural differences have a significant impact on machining performance, including surface finish, cutting forces and tool wear, highlighting the importance of material microstructure in determining machining outcomes.
- 2. In SEM analysis of milling tools, wrought Ti6Al4V showed a more evident adhesive layer on tool edges compared to SLM Ti6Al4V, attributed to higher hardness and thinner grains of SLM Ti6Al4V, which resist adhesion better. The larger, ductile  $\alpha$  and  $\beta$  grains in wrought Ti6Al4V led to increased tool wear, evident by more substantial chip welding on the rake face compared to SLM Ti6Al4V.
- 3. At higher feed rates, wrought Ti6Al4V chips become shorter with side cracks, while at lower rates, they have serrated, crack-free edges. SLM Ti6Al4V produces longer, narrower chips, reflecting the dominant in shearing over ploughing due to its microstructure.
- 4. The micro-milling study on Ti6Al4V emphasizes the critical role of material microstructure in controlling burr minimization. At a feed

- rate of 4 µm/tooth, SLM-processed Ti6Al4V produced fewer burrs than wrought Ti6Al4V. The SLM with acicular  $\alpha'$  martensite in an HCP matrix reduced burr width by 71.6% on the down-milling face, indicating superior machining performance due to its inherent brittleness and high hardness. Equiaxed grain structure and intergranular  $\beta$  phases of wrought Ti6Al4V resulted in increased plastic deformation and larger burrs, especially at 1 µm/tooth due to increased ploughing.
- 5. The SLM Ti6Al4V demonstrated a superior surface finish with minimal defects, achieving a surface roughness of 19.5–52.1 nm, significantly outperforming wrought Ti6Al4V, which ranged from 23.2 to 56.9 nm. This enhanced surface quality is directly linked to the microstructural specifics of SLM Ti6Al4V, characterized by increased hardness and reduced ductility, effectively inhibiting adhesion and promoting a better surface finish.

#### CRediT authorship contribution statement

**Muhammad Rehan:** Conceptualization, Data curation, Formal analysis, Investigation, Methodology, Visualization, Writing – original draft. **Te Zhao:** Investigation, Writing – original draft. **Wai Sze Yip:** Conceptualization, Supervision, Writing – review & editing. **Sandy Suet To:** Funding acquisition, Project administration, Supervision, Resources.

#### Availability of data and material

Available on the request from corresponding author.

#### Declaration of competing interest

The authors declare that they have no known competing financial interests or personal relationships that could have appeared to influence the work reported in this paper.

#### Acknowledgement

The work described in this paper was partially supported by the ITF Mainland-Hong Kong Joint Funding Scheme (MHKJFS) under the Innovation and Technology Commission (Project No. MHP/051/22), a grant from the Research Grants Council of the Hong Kong Special Administrative Region, China (Project No. PolyU 15221322). The authors would also like to express their sincere thanks to the funding support to the State Key Laboratories in Hong Kong from the Innovation and Technology Commission (ITC) of the Government of the Hong Kong Special Administrative Region (HKSAR), China and Research Committee of The Hong Kong Polytechnic University (No. RHD5).

#### References

- Ni C, et al. Effect of material anisotropy on ultra-precision machining of Ti-6Al-4V alloy fabricated by selective laser melting. J Alloys Compd 2020;848:156457.
- [2] Rehan M, He T, Khalil AK, Tahir D, Yip WS, To SS. Experimental investigation of the micro-milling of additively manufactured titanium alloys: Selective laser melting and wrought Ti6Al<sub>4</sub>V. Chinese J Mech Eng 2024;37(1):1–13.
- [3] Airao J, Kishore H, Nirala CK. Comparative analysis of tool wear in micro-milling of wrought and selective laser melted Ti6Al4V. Wear 2023;523:204788.
- [4] Lizzul L, et al. Influence of additive manufacturing-induced anisotropy on tool wear in end milling of TiGAI4V. Tribol Int 2020:146:106200.
- [5] de Oliveira Campos F, et al. The influence of additive manufacturing on the micromilling machinability of Ti6Al4V: a comparison of SLM and commercial workpieces. J Manuf Process 2020;60:299–307.
- [6] Ji H, et al. Microstructure and machinability evaluation in micro milling of selective laser melted Inconel 718 alloy. J Mater Res Technol 2021;14:348–62.
- [7] Al-Rubaie KS, et al. Machinability of SLM-produced Ti6Al4V titanium alloy parts. J Manuf Process 2020:57:768–86
- [8] Chen N, et al. Advances in micro milling: from tool fabrication to process outcomes. Int J Mach Tool Manufact 2021;160:103670.
- [9] Awual MR. A facile composite material for enhanced cadmium (II) ion capturing from wastewater. J Environ Chem Eng 2019;7(5):103378.

- [10] Abbas K, Znad H, Awual MR. A ligand anchored conjugate adsorbent for effective mercury (II) detection and removal from aqueous media. Chem Eng J 2018;334: 432–43.
- [11] Wang P, et al. Machinability analysis of micro-milling thin-walled Ti-6Al-4V micro parts under dry, lubrication, and chatter mitigation conditions. Proc IME B J Eng Manufact 2024;238(1–2):335–46.
- [12] Rehan M, et al. Experimental investigation of the influence of wire offset and composition on complex profile WEDM of Ti6Al4V using trim-pass strategy. Int J Adv Des Manuf Technol 2023;127(3):1209–24.
- [13] Khalil AK, et al. A novel magnetic field assisted diamond turning of Ti-6Al-4 V alloy for sustainable ultra-precision machining. Mater Today Commun 2023;35:105829.
- [14] Usman M, et al. An in-depth evaluation of surface characteristics and key machining responses in WEDM of aerospace alloy under varying electric discharge environments. Int J Adv Des Manuf Technol 2023;124(7):2437–49.
- [15] Liu S, Shin YC. Additive manufacturing of Ti6Al4V alloy: a review. Mater Des 2019;164:107552.
- [16] Rehan M, Yip WS, To SS. Experimental investigation of microstructure, tool wear, and burr formation of micro-milling of selective laser melting Ti6Al4V. In: Seventh international Conference on mechanical manufacturing and Industrial engineering (MMIE 2024): 2024. SPIE.
- [17] Manjunath K, et al. Simulation-based investigation on ultra-precision machining of additively manufactured Ti-6Al-4V ELI alloy and the associated experimental study. Proc IME B J Eng Manufact 2024;238(10):1554–67.
- [18] Yang J, et al. Effect of crystallographic orientation on mechanical anisotropy of selective laser melted Ti-6Al-4V alloy. Mater Char 2017;127:137–45.
- [19] Wu M-W, Lai P-H, Chen J-K. Anisotropy in the impact toughness of selective laser melted Ti-6Al-4V alloy. Mater Sci Eng, A 2016;650:295-9.
- [20] Yasa E, Deckers J, Kruth JP. The investigation of the influence of laser re-melting on density, surface quality and microstructure of selective laser melting parts. Rapid Prototyp J 2011;17(5):312–27.
- [21] Chen L, et al. Anisotropic response of Ti-6Al-4V alloy fabricated by 3D printing selective laser melting, Mater Sci Eng, A 2017;682:389–95.
- [22] Simonelli M, Tse YY, Tuck C. Effect of the build orientation on the mechanical properties and fracture modes of SLM Ti-6Al-4V. Mater Sci Eng, A 2014;616:1-11.
- [23] Wilson-Heid AE, et al. Quantitative relationship between anisotropic strain to failure and grain morphology in additively manufactured Ti-6Al-4V. Mater Sci Eng, A 2017;706;287–94.
- [24] Rafi H, et al. Microstructures and mechanical properties of Ti6Al4V parts fabricated by selective laser melting and electron beam melting. J Mater Eng Perform 2013;22:3872–83.
- [25] Antonysamy AA, Meyer J, Prangnell P. Effect of build geometry on the β-grain structure and texture in additive manufacture of Ti6Al4V by selective electron beam melting. Mater Char 2013;84:153–68.
- [26] Lizzul L, et al. Anisotropy effect of additively manufactured Ti6Al4V titanium alloy on surface quality after milling. Precis Eng 2021;67:301–10.
- [27] Oyelola O, et al. On the machinability of directed energy deposited Ti6Al4V. Addit Manuf 2018;19:39–50.
- [28] Bonaiti G, et al. Micro-milling machinability of DED additive titanium Ti-6Al-4V. Procedia Manuf 2017;10:497–509.
- [29] Sharma S, Meena A. Microstructure attributes and tool wear mechanisms during high-speed machining of Ti-6Al-4V. J Manuf Process 2020;50:345–65.
- [30] Zheng Z, et al. Microstructure and anisotropic mechanical properties of selective laser melted Ti6Al4V alloy under different scanning strategies. Mater Sci Eng, A 2022;831:142236.
- [31] Bedmar J, et al. Impact of remelting in the microstructure and corrosion properties of the Ti6Al4V fabricated by selective laser melting. Coatings 2022;12(2):284.
- [32] Wang J, Wang Y, Shi J. Solid-state diffusion joining of Ti6Al4V parts produced by selective laser melting: joint characteristics and bonding mechanism. Int J Adv Des Manuf Technol 2021;115(4):1037–48.
- [33] Song J, et al. Temperature sensitivity of mechanical properties and microstructure during moderate temperature deformation of selective laser melted Ti-6Al-4V alloy. Mater Char 2020;165:110342.
- [34] Karimi J, et al. Selective laser melting of Ti6Al4V: effect of laser re-melting. Mater Sci Eng, A 2021;805:140558.
- [35] Ducato A, et al. An automated visual inspection system for the classification of the phases of Ti-6Al-4V titanium alloy. In: Computer analysis of images and patterns: 15th international conference, CAIP 2013, york, UK, august 27-29, 2013, proceedings, Part II 15. Springer; 2013.
- [36] Yang J, et al. Formation and control of martensite in Ti-6Al-4V alloy produced by selective laser melting. Mater Des 2016;108:308–18.
- [37] Cao Z, et al. A machine learning method to quantitatively predict alpha phase morphology in additively manufactured Ti-6Al-4V. npj Comput Mater 2023;9(1): 195.
- [38] Rautio T, et al. Laser welding of selective laser melted Ti6Al4V: microstructure and mechanical properties. Mater Today Proc 2020;28:907–11.
- [39] Sallica-Leva E, et al. Ductility improvement due to martensite α' decomposition in porous Ti–6Al–4V parts produced by selective laser melting for orthopedic implants. J Mech Behav Biomed Mater 2016;54:149–58.
- [40] Vrancken B, et al. Heat treatment of Ti6Al4V produced by selective laser melting: microstructure and mechanical properties. J Alloys Compd 2012;541:177–85.
- [41] Kim Y-K, et al. Improvement in the high-temperature creep properties via heat treatment of Ti-6Al-4V alloy manufactured by selective laser melting. Mater Sci Eng, A 2018;715:33–40.
- [42] Neikter M. Microstructure and texture of additive manufactured Ti-6Al-4V. Luleå University of Technology; 2017.

- [43] Murgau CC. Microstructure model for Ti-6Al-4V used in simulation of additive manufacturing. Luleatekniska universitet; 2016.
- [44] de Formanoir C, et al. Micromechanical behavior and thermal stability of a dualphase α+ α'titanium alloy produced by additive manufacturing. Acta Mater 2019; 162:149-62
- [45] Krakhmalev P, et al. Deformation behavior and microstructure of Ti6Al4V manufactured by SLM. Phys Procedia 2016;83:778–88.
- [46] Chatterjee R, et al. Crystal plasticity-phase-field based analyses of interfacial microstructural evolution during dynamic recrystallization in a dual phase titanium alloy. Int J Plast 2024;181:104087.
- [47] Galindo-Fernández M, et al. A microstructure sensitive model for deformation of Ti-6Al-4V describing Cast-and-Wrought and Additive Manufacturing morphologies. Mater Des 2018;160:350–62.
- [48] Lütjering G, et al. Commercially pure (CP) titanium and alpha alloys. Titanium; 2003. p. 149–75.
- [49] Hayes BJ. Characterization of Ti-6Al-4V produced via electron beam additive manufacturing. University of North Texas; 2015.
- [50] Shahsavari M, et al. Corrosion evaluation of Ti-6Al-4V manufactured by electron beam melting in Ringer's physiological solution: an in vitro study of the passive film. J Appl Electrochem 2022;52(6):1003-19.
- [51] Altan CL, et al. Enhancement of thermal conductivity upon application of magnetic field to Fe3O4 nanofluids. J Appl Phys 2011;110(9).
- [52] Mironov S, et al. Microstructure evolution during warm working of Ti–6Al–4V with a colony- $\alpha$  microstructure. Acta Mater 2009;57(8):2470–81.
- [53] Beladi H, Chao Q, Rohrer GS. Variant selection and intervariant crystallographic planes distribution in martensite in a Ti-6Al-4V alloy. Acta Mater 2014;80: 478-89.
- [54] Yan Q, et al. Comparison study on microstructure and mechanical properties of Ti-6Al-4V alloys fabricated by powder-based selective-laser-melting and sintering methods. Mater Char 2020;164:110358.
- [55] Qiu C, Adkins NJ, Attallah MM. Microstructure and tensile properties of selectively laser-melted and of HIPed laser-melted Ti-6Al-4V. Mater Sci Eng, A 2013;578: 230-9

- [56] Wauthle R, et al. Effects of build orientation and heat treatment on the microstructure and mechanical properties of selective laser melted Ti6Al4V lattice structures. Addit Manuf 2015;5:77–84.
- [57] Xu W, et al. Additive manufacturing of strong and ductile Ti-6Al-4V by selective laser melting via in situ martensite decomposition. Acta Mater 2015;85:74–84.
- [58] Dornfeld D, Min S, Takeuchi Y. Recent advances in mechanical micromachining. CIRP annals 2006;55(2):745–68.
- [59] Aramcharoen A, Mativenga P. Size effect and tool geometry in micromilling of tool steel. Precis Eng 2009;33(4):402–7.
- [60] Dere EG, et al. Effect of niobium and grain boundary density on the fire resistance of Fe-C-Mn steel. Scripta Mater 2013;68(8):651-4.
- [61] Tian S, et al. The mechanism of anisotropic micro-milling properties in additively manufactured Ti-6Al-4V alloy. J Mater Process Technol 2023;322:118190.
- [62] Mamedov A, Lazoglu I. Thermal analysis of micro milling titanium alloy Ti-6Al-4V. J Mater Process Technol 2016;229:659-67.
- [63] Pratap T, Patra K, Dyakonov AA. Modeling cutting force in micro-milling of ti-6al-4 v titanium alloy. Procedia Eng 2015;129:134–9.
- [64] Ahmadi M, et al. Microstructure effects on process outputs in micro scale milling of heat treated Ti6Al4V titanium alloys. J Mater Process Technol 2018;252:333–47.
- [65] Nakayama K, Arai M. Burr formation in metal cutting. CIRP Annals 1987;36(1): 33–6.
- [66] Chen Z, et al. Comparative study on micro-milling machinability of titanium alloys prepared by different processes: forging process, additive manufacturing process and heat-treatment process. Precis Eng 2024.
- [67] Wu X, et al. Investigation on surface quality in micro milling of additive manufactured Ti6Al4V titanium alloy. J Manuf Process 2023;101:446–57.
- [68] Airao J, et al. Tribological performance in micro-milling of Ti6Al4V under nanofluid-based minimum quantity lubrication. Int J Interact Des Manuf 2024: 1–13.
- [69] Chen Z, et al. Comparative study on micro-milling machinability of titanium alloys prepared by different processes: forging process, additive manufacturing process and heat-treatment process. Precis Eng 2024;88:164–76.